Genomics

Molecular Cancer Research

Pathology-Driven Comprehensive Proteomic Profiling of the Prostate Cancer Tumor Microenvironment

Lisa Staunton[1], Claire Tonry[1], Rosina Lis[2], Virginia Espina[3], Lance Liotta[3], Rosanna Inzitari[1], Michaela Bowden[2], Aurelie Fabre[1,4], John O'Leary[5], Stephen P. Finn[5], Massimo Loda[2,6], and Stephen R. Pennington[1]

Abstract

Prostate cancer is the second most common cancer in men worldwide. Gleason grading is an important predictor of prostate cancer outcomes and is influential in determining patient treatment options. Clinical decisions based on a Gleason score of 7 are difficult as the prognosis for individuals diagnosed with Gleason 4+3 cancer is much worse than for those diagnosed with Gleason 3+4 cancer. Laser capture microdissection (LCM) is a highly precise method to isolate specific cell populations or discrete microregions from tissues. This report undertook a detailed molecular characterization of the tumor microenvironment in prostate cancer to define the proteome in the epithelial and stromal regions from tumor foci of Gleason grades 3 and 4. Tissue regions of interest were isolated from several Gleason 3+3 and Gleason 4+4 tumors using telepathology to leverage specialized pathology expertise to support LCM. Over 2,000 proteins were identified following liquid chromatography tandem mass spectrometry (LC-MS/MS) analysis of all regions of interest. Statistical analysis revealed significant differences in protein expression (>100 proteins) between Gleason 3 and Gleason 4 regions—in both stromal and epithelial compartments. A subset of these proteins has had prior strong association with prostate cancer, thereby providing evidence for the authenticity of the approach. Finally, validation of these proteins by immunohistochemistry has been obtained using an independent cohort of prostate cancer tumor specimens.

Implications: This unbiased strategy provides a strong foundation for the development of biomarker protein panels with significant diagnostic and prognostic potential. *Mol Cancer Res; 15(3); 281–93. ©2017 AACR.*

Introduction

Prostate cancer remains one of the leading causes of cancer morbidity and mortality in men worldwide (1). Prostate cancer is initially indicated by increased levels of prostate-specific antigen (PSA) in the blood; however, pathologic evaluation of tissue obtained at needle biopsy is essential to confirm prostate cancer diagnosis and provide data to define a patient's risk category (2). Pathologic evaluation of the prostate tumor follows the Gleason Scoring (GS) system, which is based on the observed histologic pattern of carcinoma cells in hematoxylin and eosin (H&E)–stained prostatic tissue sections, viewed under low magnification (3). The GS system is based on five basic patterns of tissue morphology (G1–5), and the ultimate histologic score, ranging from 2–10, is obtained by adding the primary grade pattern to the secondary grade pattern (4). Tumor grade as determined by Gleason score is the most important predictor of clinical outcome and the central parameter for guiding management decisions. Patients with a low Gleason score ($G \leq 6$) are considered to have low-risk disease and therefore suitable for an active surveillance program, whereas patients with a high Gleason score (G8–G10) are considered to have high-risk disease and generally referred for adjuvant therapy or radiation treatment (3). The projected outcomes for patients with G7, however, are less clear as this grade can represent either a mostly well-differentiated cancer with a lesser component of more poorly differentiated cancer (G3+4) or a mostly poorly differentiated cancer with a small component of well-differentiated cancer (G4+3). The clinical behavior of G3 tumors appears to be fundamentally different to G4 tumors, and so the clinical outcome for those diagnosed with G4+3 tumor is much worse than those who are diagnosed with G3+4 tumor (5). However, treatment decisions using a simplified Gleason score of G7 fail to recognize these prognostic differences (6, 7). A modified version of the GS system has therefore been introduced in which prostate cancer tumors are graded as follows: grade group 1 ($G \leq 6$), grade group 2 (G3+4), grade group 3 (G4+3), grade group 4 (G8), and grade

[1]UCD Conway Institute of Biomolecular and Biomedical Research, University College Dublin, Dublin, Ireland. [2]Center for Molecular Oncologic Pathology, Harvard Medical School, Boston, Massachusetts. [3]Center for Applied Proteomics, George Mason University, Fairfax, Virginia. [4]Department of Histopathology, St Vincent's University Hospital, Dublin, Ireland. [5]Department of Histopathology, St. James's Hospital, Dublin, Ireland. [6]Department of Pathology, Brigham and Women's Hospital, Boston, Massachusetts.

Note: Supplementary data for this article are available at Molecular Cancer Research Online (http://mcr.aacrjournals.org/).

Corresponding Author: Stephen R. Pennington, University College Dublin, Belfield, Dublin 4, Ireland. Phone: 0035317166783; E-mail: stephen.pennington@ucd.ie

doi: 10.1158/1541-7786.MCR-16-0358

group 5 (G9–10; ref. 7). Although this revision has reportedly resulted in a more accurate grading system for prostate cancer patients, a great deal of variation remains associated with tumor sampling for Gleason grading. The current practice of extracting multiple cores from the highly heterogeneous tumor tissue means that the most aggressive areas of tumor can easily be either over- or under-represented. In addition, the discordance between GS of biopsy samples before and after prostatectomy can be as high as 30% (2).

Overall, conventional diagnosis and prognosis of prostate cancer are based on the primary tumor, and many argue that this may be inappropriate if an individual already has metastatic or non–organ-confined disease. Most treatment options for prostate cancer are designed to exclusively target the tumor itself—a strategy that is plagued by the development of resistance, conferred by the inherent genetic instability of prostate cancer. In addition to cancer epithelial cells, a primary tumor consists of nonepithelial components (blood vessels, lymph vessels, immune cells, etc.) that are collectively referred to as the tumor stroma (8, 9). Interactions between tumor epithelial and stromal tissue have a key role in promoting tumor growth and dissemination of cancer cells from the primary tumor site, leading to metastasis (8). The concept of targeting stromal support mechanisms ("anti-stromal" therapy) has emerged as an appealing alternative to current therapeutic strategies for cancer treatment (10). In addition, the stroma may also be a useful source of biomarkers to indicate disease progression and/or treatment failure (11). The National Comprehensive Cancer Network now recommends molecular testing to inform treatment decisions regarding localized prostate cancer. Indeed, the ProMark assay by Metamark has demonstrated the clinical utility of multiplexed measurements of protein changes for predicting prostate cancer aggressiveness (12). The key aims of this study were therefore to (i) investigate, at the protein level, the molecular differences in the tumor microenvironment of G3 and G4 tumor tissue, (ii) identify discriminatory proteins between G3 and G4 that could be used as markers to aid diagnosis of G3+4 or G4+3 and monitor progression to metastatic disease, and (iii) identify targets which could be used to intervene therapeutically.

Laser capture microdissection (LCM) is an extremely powerful technology used for the enrichment of specific cell populations from heterogeneous tissue sections (13). Advancements that have been made in proteomics technology mean that it is now feasible to profile up to 3,000 proteins from limited sample material (14, 15). Herein, we describe an optimized "micropathomics" workflow that supports telepathology-driven proteomics for comprehensive profiling of the prostate cancer tumor microenvironment. Although it would have been desirable to analyze regions of G3 and G4 tumor from within the same G7 tumor, acquisition of sufficient G3 and G4 material from G7 tumor tissue would be challenging—not least because scoring of G7 tumor is highly subjective. As such, tumor material from pure G6 (G3+3) and G8 (G4+4) gave the best chance of acquiring sufficient material from the correct tumor grade. In addition, analysis of the potentially more extreme differences between G3 and G4 (from G3+3 and G4+4) would allow identification of the most clinically relevant protein changes that might be further evaluated in tissue from patients with G3+4 versus G4+3. Fresh-frozen tissue derived from G3+3 and G4+4 patients was thus used to provide sufficient LCM material for advanced LC-MS/MS analysis and comprehensive molecular characterization of the G3 and G4 tumor microenvironment. Statistical comparisons of protein expression changes in G3 versus G4 epithelia revealed differential expression of 120 proteins, which mapped onto a number of different pathways. Furthermore, it was found that a much greater number of proteins (326) were differentially expressed between epithelial and stromal regions of G4 tumor as compared with G3 tumor—with only a small (14.9%) overlap in these protein changes. Although these changes were not further explored as part of this study, they are likely to be informative of the signaling activity between tumor stroma and epithelia that support and promote prostate cancer progression. Indeed, their functional significance is to be explored further, including with combined analysis of RNAseq data obtained from adjacent tissue sections that were also subject to LCM. To evaluate the potential relevance of significantly changing proteins between G3 and G4 epithelia, a subset (selected under stringent criteria) were evaluated by immunohistochemistry (IHC)-based analysis of biopsy samples from a separate sample cohort of 133 prostate cancer patients. Overall, this study provides a rich protein dataset from LCM material that can be used to address a fundamental question in prostate cancer—namely, do cellular subtypes within the tumor microenvironment show distinct patterns of protein expression that could offer mechanistic insight into tumor initiation and progression.

Materials and Methods

Tissue samples

Prostate tumor tissue specimens were obtained from the Arthur and Linda Gelb Center for Translational Research Prostate Tissue Bank at the Dana-Farber Cancer Institute, Boston, MA. All patients had consented to have clinical data collected prospectively and to provide all prostate tissue obtained during biopsy and surgery (16). Snap-frozen tissue was mounted on a tissue holder with the assistance of Tissue-Tek O.C.T. Compound (Sakura; SAK 4583), and fresh-frozen tissue sections were cut onto individual glass slides; 5-μm tissue sections were stained with H&E for pathologic review, and 8-μm tissue sections were stained with the Histogene LCM Frozen Section Staining Kit (Life Technologies; KIT0401) for downstream LCM. Protease inhibitors (Roche; 04693124001) were added to all water containing solutions. LCM slides were allowed to air dry, and LCM was performed immediately and completed within 1 hour of staining.

LCM and short-range SDS-PAGE

Tissue microdissection was conducted using an Arcturus microdissection instrument (AXT1931; Molecular Devices) guided by an expert pathologist. Reviewed and annotated H&E slides were viewed digitally using Spectrum software (Fig. 1). All available regions of interest (ROI) were acquired for each section and captured onto CapSure Macro LCM caps (Life Technologies; LCM0211). LCM area volumes as well as the number of laser shots were documented, and images of predissected LCM slides, acquired microdissected tissue on MacroCap, and post-LCM slides were taken for full documentation. Immobilized microdissected cells on the macro caps were mounted securely into the opening of 0.5 mL Eppendorf tubes and stored at −80°C until further processing. For protein extraction from each ROI, 10 μL of lysis buffer (7 mol/L Urea,

2 mol/L Thiourea, 2 mol/L CHAPS, 100 mmol/L DTT, Complete Mini Protease Inhibitor Cocktail) was added to an LCM cap of that ROI and used to serially extract from all remaining caps of the same ROI. The resulting pooled protein extract for each ROI was placed in Lo-Bind 0.5 mL tubes (Sigma; Z666491) for subsequent short-range SDS-PAGE on 6% polyacrylamide gels (17). Electrophoresis was performed at 80 V for 20 minutes, or until the tracking dye fully entered the top of the resolving gel.

Protein digestion and LC-MS/MS

Concentrated protein bands were excised, washed, and digested according to an optimized method previously described by Shevchenko and colleagues (18). Peptides were dried by vacuum centrifugation, and the peptide fractions were resuspended in 1 μg/μL 0.1% TFA and prepared for LC-MS/MS analysis using C18-Stage tips according to the protocol by Rappsilber and colleagues (19). Peptides were dried down completely under vacuum at 30°C and resuspended in 1 μg/μL buffer (3% ACN/0.1% formic acid). Purified peptide samples were analyzed on a Thermo Scientific Q Exactive mass spectrometer coupled to a Dionex Ultimate 3000 (RSLCnano) chromatography system. Full details of the parameters used for LC-MS/MS analysis are included in Supplementary Data.

Bioinformatic data analysis

Raw data were *de novo* sequenced and searched against the Homosapien subset of the UniProt Swiss-Prot database (2014_11 version) using the search engine PEAKS Studio 6 (version 6). Subsequently, the raw data flies were processed through the Andromeda search engine via MaxQuant (V.1.2.7.4) software with the same parameter settings as Peaks Studio 6. The label-free quantification values were generated with a minimum of two peptides required per protein.

Full details of the search parameters used are included in Supplementary Data.

Statistical analysis

Comparison of differential protein abundance between tumor ROIs was determined using % coefficient of variation (CV) and fold-change analysis. The % CV across four sample replicates (SR) was used to map variation in the experimental samples. Differentially expressed proteins were determined with >2 SD separation. Following manual interrogation of the data, the .txt file generated by Andromeda processing of the raw data was uploaded onto Perseus version 1.5.0.6. Data were filtered to remove reverse phase proteins and proteins only identified by site. Statistically significant changes in protein expression between "benign epithelial and tumor epithelial" and "benign stromal and tumor stromal" were assessed using one-way ANOVA, Student *t* test, principal component analysis (PCA), and hierarchical clustering in the Perseus software.

Pathway analysis

Analysis of functional pathways was carried out using Ingenuity Pathway Analysis (IPA) Ingenuity Systems software package.

IHC analysis

For IHC staining, antibodies were purchased for the following proteins: U2 small nuclear ribonucleoprotein A (HPA045622), Bifunctional epoxide hydrolase 2 (HPA023094), Nucleolin (HPA23981), and Ras-related protein Rab-3D (CAB018067). Formalin-fixed, paraffin-embedded adipose tissue samples were deparaffinized and hydrated using xylene and alcohol. Heat antigen retrieval was performed for 20 minutes at 97°C in pH 6 buffer (Dako) in the Dako PT link. Sections were processed using the Dako Envision FLEX Rabbit and Mouse Linker Kits (Dako) according to the manufacturer's instructions on the automated Dako 48 link Autostainer. Sections were incubated with primary antibodies at room temperature, followed by polyclonal rabbit anti-rat/anti-mouse secondary antibodies (Dako). Sections were detected with DAB (x2 5 min) and counterstained with hematoxylin. Isotypes were run in parallel as well as a negative control with primary antibody omitted and positive controls (breast carcinoma for RAB3D, NCL and SNRPA1, and normal lung for EPHX2) to assess for specific antigenicity. For semiquantitative analysis, slides were scored 1 to 3 (see Fig. 4) in normal prostatic tissue and various grades of prostatic adenocarcinoma. Photographs were taken using a Nikon camera (software NIS elements F3.0).

Results

A micropathology approach for LCM for proteomic analysis

Effective proteomic profiling of limited quantities of protein, extracted from defined ROIs routinely acquired using LCM, has been established previously (20). For this study, the micropathomic workflow described in Fig. 1 was applied to obtain tumor cells from annotated ROIs from patient tumor samples via LCM. Exclusive Gleason score 6 ($n = 4$) and Gleason score 8 ($n = 4$) patients were selected for this study to provide samples of extreme Gleason 3 (G3) and Gleason 4 (G4) tumor regions, respectively. In total, 8 patient samples were processed for LCM, and 15 sections were taken from each patient tissue block. Stromal regions were selected from tissue immediately adjacent to the tumor region. Sections (5 μm) from the top, middle, and tail end were stained with H&E to be used for slide annotation and documentation (Fig. 1). For advanced LC-MS/MS, a total of 12 sections (8-μm-thick) were taken from between each of the H&E-stained sections and subject to LCM (Fig. 1). LCM acquired approximately 2,500 to 10,000 cells from each tumor ROI. In total, LCM was performed on 96 tumor tissue sections to isolate sufficient cell material from the following ROIs: G3 tumor epithelium (G3E), G3 associated stroma (G3S), G4 tumor epithelium (G4E), and G4 associated stroma (G4S). This process took approximately 6 weeks (Fig. 1). The rigorous and systematic documentation approach for recording all tissue images and LCM reports supported verification of the identity of captured cells. The numbers of cells captured were estimated using methods as described elsewhere (ref. 21; Fig. 1). For proteomic analysis, LCM-captured tissue sections for ROIs were lysed, and the region-specific lysates were pooled to generate four replicate pools of G3S, G3E, G4S, and G4E. These lysates were prepared for advanced LC-MS/MS analysis using short-range SDS-PAGE. Following short-range SDS-PAGE, gel bands were cut and digested with trypsin, yielding between 1 and 12 μg/μL peptide material for all replicate pools.

LC-MS/MS analysis of LCM material

For LC-MS/MS analysis of the digested replicate pools, samples were stage-tipped (prepared in-house with C18 discs) to purify the peptide material. Based on the protein quantification

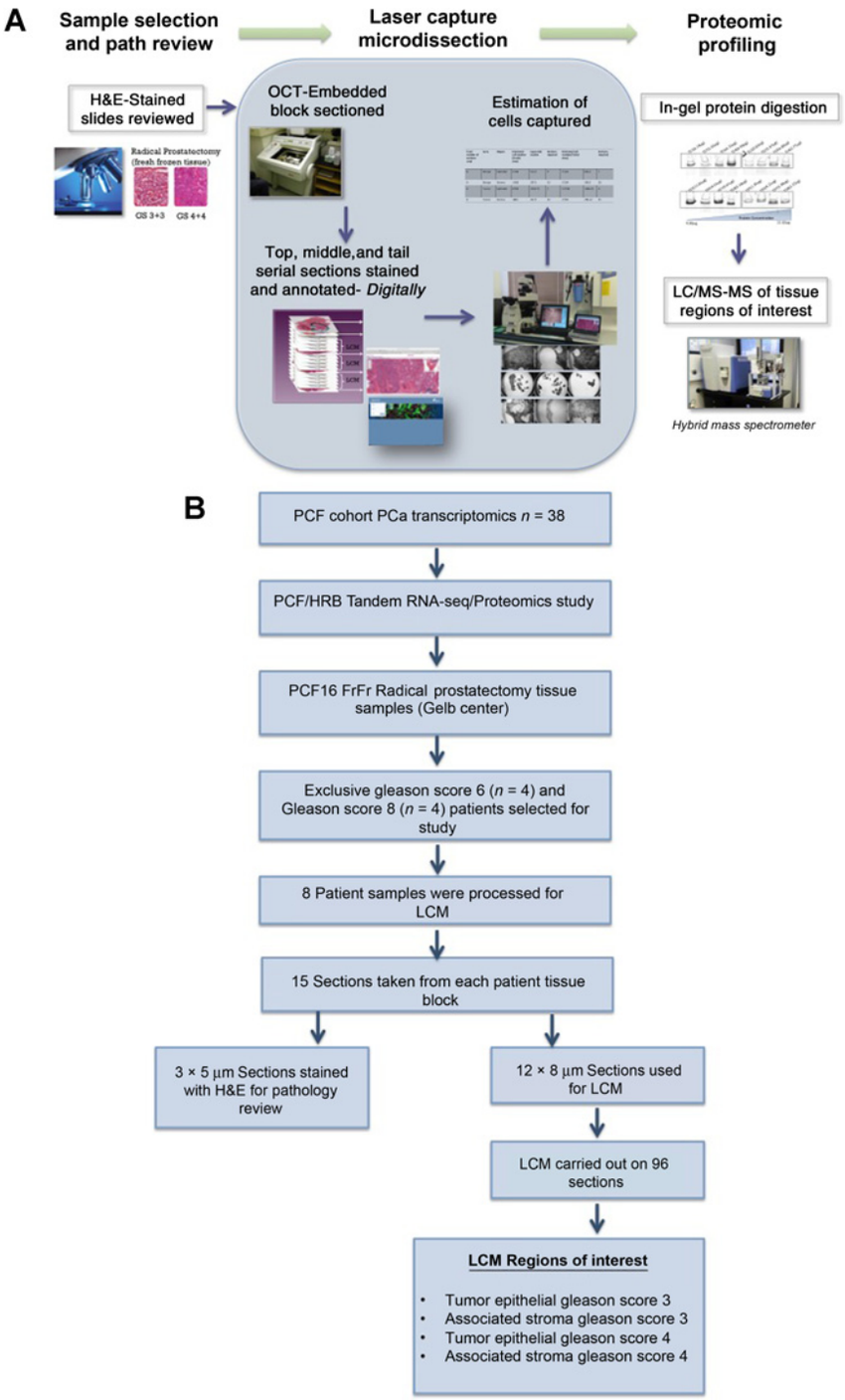

Figure 1.
Workflow for LCM coupled with advanced LC-MS/MS proteomic analysis.

of in-gel–digested replicate samples, a maximum of 1 µg peptide material was generated for LC-MS/MS analysis to ensure accurate proteomic profiling of all four replicates generated for each ROI. For all samples, total dried-down peptide material (1 µg) was reconstituted in 6 µL buffer solution (3% v/v ACN/0.1% v/v formic acid) and analyzed on a Q Exactive mass spectrometer. For some of the ROIs, there was insufficient material to allow for repeat analysis, and so experimental parameters were considered carefully. A number of preliminary experiments were performed, and chromatography conditions for LC-MS analysis of the precious LCM material were selected to ensure that a complete MS/MS dataset could be acquired from all samples. Reproducibility of the LC-MS/MS analysis was evaluated by including a crude protein lysate from benign prostate tissue (control) in the experimental analysis. This sample served as both a technical replicate to

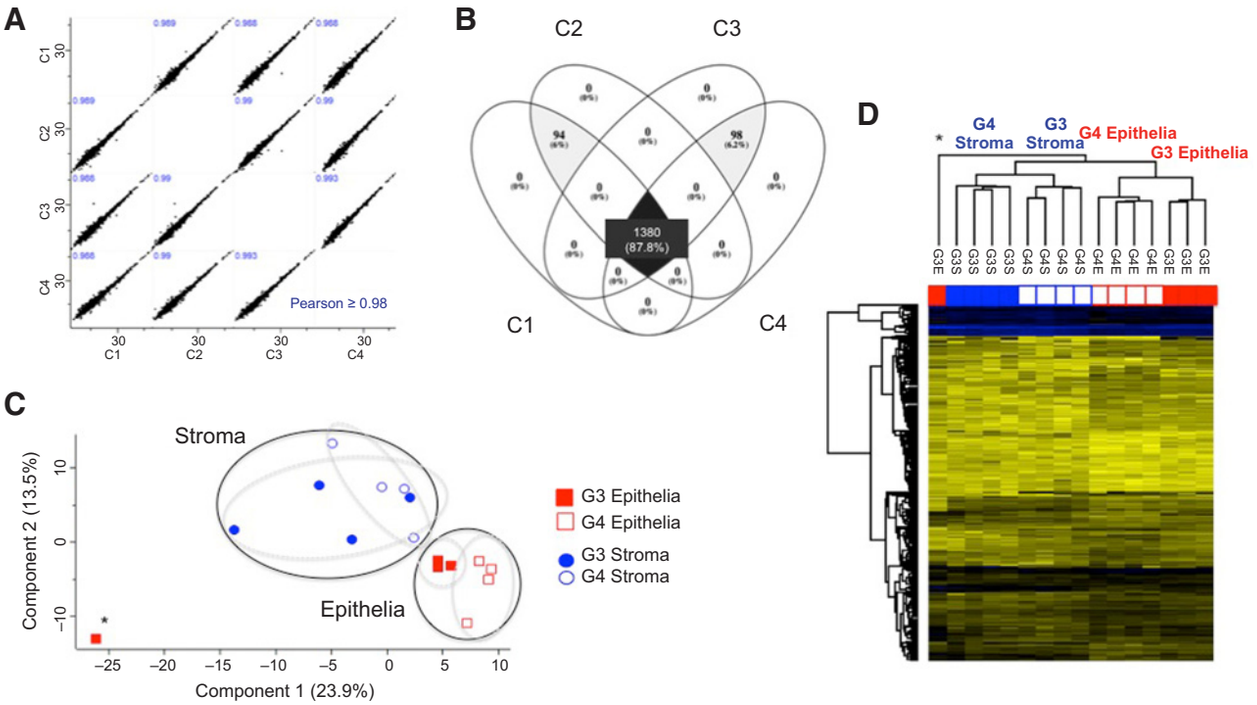

Figure 2.

LC-MS/MS analysis of ROIs. Technical reproducibility was confirmed with high Pearson correlation (≥0.98) between the control samples (**A**) and a large overlap between the proteins identified in each control sample (**B**). PCA analysis (**C**) and hierarchical clustering (**D**) revealed significant differences in protein expression between epithelial and stromal tissues within both G3 and G4 tissues—apart from one outlier. Significant differences were also observed in the protein expression between G3 and G4 stromal and G3 and G4 epithelial tissues (**C** and **D**).

assess technical reproducibility and an SR to assess the reproducibility of the process of sample preparation. The run order, which included four replicates of each ROI, was randomized to minimize any instrument-related bias, with the control sample being analyzed at the beginning, middle, and end of the run. Following MS data acquisition, raw data were uploaded onto PEAKS software (version 6) to assess the number of protein identifications in each sample. The overall micropathomic workflow resulted in the identification of over 2,000 proteins across all experimental samples (≥2 uniquely mapping peptides, minimum peptide length = 7 aa, ≤ 2 missed cleavages and protein FDR = 0.01,). Data from the control sample confirmed reproducibility of the analysis, as indicated by a Pearson correlation of ≥0.98 (Fig. 2A). The proteins identified in each of the control samples are summarized in the Venn diagram displayed in Fig. 2B. Notably, the varied amount of protein material which could be successfully extracted from each of the ROI-pooled samples was not reflected in the numbers of proteins identified following LC-MS/MS analysis of approximately 1 μg of peptide material from each ROI pool (Fig. 2B).

Proteomic characterization of morphologically distinct tumor regions

Proteomic characterization of morphologically distinct tumor regions was conducted using Perseus (version 1.5.0.6) software. As an initial step, the data were filtered to remove proteins categorized as "reverse" and "only identified by site." Proteins classified as "contaminant" were retained as these can also be subject to alterations in cancer—as has been observed for keratins (22). Data were filtered further to retain three valid values (of a possible four) in at least one sample group—G3E, G4E, G3S, and G4S—so as not to exclude any proteins that might only be present in one sample group. Missing values were replaced by normal distribution, and the data were normalized based on the standard normal distribution (z-score). Variances in protein expression across all sample groups were assessed via ANOVA ($P \leq 0.05$) analysis (Fig. 2D). With the exception of one outlier, PCA of the data showed a clear overall separation between stromal and epithelial tissues (Fig. 2C and D). It is worth noting that this anomaly was not associated with a difference in starting protein concentration as determined following in-gel protein digestion. Moreover, the PCA analysis demonstrates clear differentiation between G3 and G4 tumors in both epithelial and stromal regions (Fig. 2C and D). Further assessment of differential protein expression between groups (G3E, G3S, G4E, and G4S) was achieved by the Student *t* test (Permutation-based, FDR 0.05) analysis. The numbers of differentially expressed proteins between each tumor grade (G3 vs. G4) and each tissue region (stromal vs. epithelial) are displayed in Table 1. The full list of significantly changing proteins is included in Supplementary Table S1.

Comparative analysis of G3 and G4 tumor regions

IPA highlighted the molecular functions most significantly up- or downregulated based on the expression of significantly

Table 1. Numbers of differentially expressed proteins between morphologically distinct tumor regions

Analysis	Number of significantly changing proteins	Upregulated	Downregulated
G3E vs. G3S	84	39	45
G4E vs. G4S	326	137	189
G3E vs. G4E	120	55	65
G3S vs. G4S	78	41	37

NOTE: The name and accession numbers of all significantly changing proteins are listed in Supplementary Table S1.
Abbreviations: G3E, Gleason grade 3 epithelia; G4E, Gleason grade 4 epithelia; G3S, Gleason grade 3 stroma; G4S, Gleason grade 4 stroma.

changing proteins between G3 epithelia and G4 epithelia (Table 2). For both G3E and G4E, differentially expressed proteins were shown to be involved in regulation of the cell cycle, proliferation, gene expression, and metabolism. The key difference was found to be in RNA processing—especially in the expression of mRNA splicing proteins. Notably, splice isoforms of Kinectin were found to upregulated in epithelial tissue form both GS3 and GS4 tumors. The same splice isoforms of Kinectin have previously been identified as one of six overexpressed splice isoforms associated with $HER2^+/ER^-/PR^-$ breast cancer and are thought to have a role in $HER^+/ER^-/PR^-$ tumor progression (23). The proteins significantly changed between the associated stroma of Gleason 3 and Gleason 4 tumor regions were also analyzed. Here, it was observed that for both tumor grades, differential expression occurred in key proteins involved in cell death and survival and metabolism. The most significant molecular differences between G3 stroma and G4 stroma were in the expression of immune response proteins and in cell-to-cell signaling proteins which were found to be increased in G4 stroma (Table 2). This analysis also highlighted the increased expression of Tubulin alpha-1A chain in G4 stroma as compared with G3 stroma. This protein was recently reported by Webber and colleagues as being a potential "stromal" biomarker of prostate cancer (11). Another well-documented protein associated with aggressive prostate cancer—zinc-alpha-2-glycoprotein—was also found to be upregulated in the G4 stroma as opposed to the G3 stroma (24–26). All proteins associated with the changes in molecular activity described above, along with their fold change, are listed in Table 2 of Supplementary Data.

Table 2. Molecular functions associated with differentially expressed proteins in G3 and G4 epithelial and stromal tissues

Molecular function[a]	Regulation	
G3 epithelia versus G4 epithelia	**G3E**	**G4E**
RNA posttranslational modification: mRNA splicing		↓
Cell cycle	↓	↓
Protein synthesis	↓	↑
Cellular assembly and organization		↑
Carbohydrate metabolism	↑	↓
G3 stroma versus G4 stroma	**G3S**	**G4S**
Cell-to-cell signalling		↑
Cell death and survival	↓	↑
Protein synthesis		↑
Cell morphology	↑	
Cellular assembly and organization	↑	
G3 epithelia versus G3 stroma	**G3E**	**G3S**
Cellular assembly organization	↓	↑
Cell-to-cell signaling and interaction	↓	↑
Carbohydrate metabolism	↑	
Cell cycle	↑	
G4 epithelia versus G4 stroma	**G4E**	**G4S**
Free radical scavenging	↑	↓
Cell growth, proliferation, and cell death	↑	
RNA posttranslational modification	↑	
Cellular assembly and organization		↑
Immune response		↑

[a]The significantly changing proteins contributing to the up- or downregulation of the molecular functions described in this table are listed in Supplementary Table S2.

Another aim of this study was to identify novel targets that could potentially be used for therapeutic intervention. Therefore, the molecular composition of epithelial versus associated stromal tissue was further investigated for both Gleason 3 and Gleason 4 tissue regions. Notably, there were a much greater number of proteins (326) found to be significantly changed between epithelial and stromal regions of G4 tumor as opposed to G3 tumor (84 proteins; Table 1). Two of these—HSPA9 and YBOX1—are measured as part of the ProMark 8-protein signature which has been reported as a powerful, independent risk predictor for prostate cancer (12, 27). In the G3 microenvironment, there was found to be a significant increase in proteins involved in cell cycle and carbohydrate metabolism in the epithelial tissue. Comparative analysis of the G4 microenvironment revealed a significant increase in proteins associated with cell proliferation and RNA posttranslational modification in epithelial tissue, whereas heightened expression of immune response proteins was observed in the stromal tissue (Table 2).

Evaluation of discriminatory protein markers for G3+4 and G4+3

The molecular composition of G3 epithelia versus that of G4 epithelial may be of significant importance to the progression of prostate cancer. As such, proteomic profiling of G3 tumor regions was undertaken via advanced LC-MS/MS analysis. As described previously, the data were first processed through MaxQuant (version 1.5.2.8) software, and further comparisons of G3 versus G4 tumors were undertaken using Perseus (version 1.5.2.6) and IPA (version 01–04) software. Statistical analysis of G3 versus G4 epithelia in Perseus software identified 120 differentially expressed proteins of which a subset was shown to have a key role in the regulation of distinct molecular functions which show differential regulation between G3 and G4 epithelia. To ensure that proteins brought forward for further evaluation were truly significant, the data were further interrogated with two data analysis workflows by three independent researchers with the researchers blinded to each other's results. Both workflows incorporated ANOVA and Student *t* test analysis (Supplementary Fig. S2). This led to the identification of 29 proteins that were consistently found to show a significant change in expression between G3 and G4 epithelia (Table 3). A number of steps were taken to guide selection of a more refined number of proteins to be evaluated using IHC (Fig. 3). The Human Protein Atlas was fundamental in this process. The Human Protein Atlas portal is a publicly available database that provides information—through high-resolution images—of the spatial distribution of proteins in a number of different normal human tissues, cancer types, and human cell lines (www.proteinatlas.org). All 29 proteins showing a consistent significant change between G3 and G4 epithelia were queried through ProteinAtlas to assess (i) their evidence as a protein, (ii) whether they are routinely expressed in prostate tissue/prostate cancer, (iii) whether appropriate antibodies are available for IHC analysis of protein expression, and (iv) the

Table 3. Shortlist of significantly changing proteins between G3E and G4E and associated networks

Gene names	Protein IDs	Protein names	t-test difference	PROTEIN ATLAS—Ab Quality	Antibody	G4 vs. G3	IPA network
RPL28	P46779	60S ribosomal protein L28	−0.877	stain MEDIUM 9/10		↑	
RBM4	Q9BWF3	RNA-binding protein 4	−0.622	stain MEDIUM 2/9		↑	
RPL5	P46777	60S ribosomal protein L5	−0.614	stain MEDIUM 9/11		↑	
NCL	**P19338**	**Nucleolin**	**−0.608**	**stain HIGH 10/11**	**HPA023981**	↑	**Molecular transport, protein synthesis and trafficking, cellular assembly and organization, gene expression, infectious disease**
ATP5H	O75947-2	ATP synthase subunit d, mitochondrial	−0.584	stain HIGH 6/12	HPA048459	↑	Nucleic acid metabolism, small-molecule biochemistry, DNA replication, recombination, and repair
THRAP3	Q9Y2W1	Thyroid hormone receptor–associated protein 3	−0.521	stain HIGH 4/8		↑	Protein synthesis, gene expression, hematologic disease, RNA posttranscriptional modification
H1FX	Q92522	Histone H1x	−0.495	stain MEDIUM 5/9		↑	
SNRPA1	**P09661**	**U2 small nuclear ribonucleoprotein A**	**−0.470**	**stain HIGH 9/9**	**HPA045622**	↑	**RNA posttranscriptional modification, infectious disease, renal and urological disease**
RPL23	P62829	60S ribosomal protein L23	−0.440	stain MEDIUM 9/12		↑	
PPIB	P23284	Peptidyl-prolyl cis-trans isomerase B	−0.400	stain MEDIUM 11/11		↑	
TPD52	P55327-2	Tumor protein D52	−0.384	stain HIGH 6/12	HPA028427	↑	Cellular function and maintenance, cellular assembly and organization, infectious disease, drug metabolism, endocrine system development and function, and lipid metabolism
HNRNPL	P14866	Heterogeneous nuclear ribonucleoprotein L	−0.360	stain HIGH 11/12	HPA052661	↑	Protein synthesis, infectious disease, RNA posttranscriptional modification
HNRNPUL1	Q9BUJ2-4	Heterogeneous nuclear ribonucleoprotein U-like protein 1	−0.348	stain MEDIUM 9/12		↑	
RALY	Q9UKM9-2	RNA-binding protein Raly	−0.345	stain HIGH 2/11		↑	Protein synthesis, infectious disease, RNA posttranscriptional modification
RPL10A	P62906	60S ribosomal protein L10a	−0.302	stain MEDIUM 6/9		↑	
APEH	P13798	Acylamino-acid-releasing enzyme	+0.365	stain MEDIUM 4/11		↓	
GOT1	P17174	Aspartate aminotransferase, cytoplasmic	+0.367	Not available		↓	
USP14	P54578-2	Ubiquitin carboxyl-terminal hydrolase 14	+0.418	stain HIGH 8/10	HPA001308	↓	DNA replication, recombination, and repair, energy production, nucleic acid metabolism
RAB3D	**O95716**	**Ras-related protein Rab-3D**	**+0.487**	**stain HIGH 10/11**	**CAB018067**	↓	**Cellular function and maintenance, cellular assembly and organization, infectious disease**
DCXR	Q7Z4W1	L-xylulose reductase	+0.533	stain LOW 2/10		↓	
DPT	Q07507	Dermatopontin	+0.546	Not available		↓	
PPL	O60437	Periplakin	+0.597	stain MEDIUM		↓	
QDPR	P09417	Dihydropteridine reductase	+0.624	stain MEDIUM 1/11		↓	
SOD3	P08294	Extracellular superoxide dismutase [Cu-Zn]	+0.627	stain MEDIUM 4/10		↓	
OLFML3	Q9NRN5	Olfactomedin-like protein 3	+0.848	9/11 not detected		↓	
EPHX2	**P34913**	**Bifunctional epoxide hydrolase 2**	**+0.964**	**stain HIGH 12/12**	**HPA023094**	↓	
EMILIN1	Q9Y6C2	EMILIN-1	+0.965	12/12 not detected		↓	Molecular transport, protein trafficking, cellular assembly, and organization
FMOD	Q06828	Fibromodulin	+1.154	Not available		↓	
GDF15	Q99988	Growth/differentiation factor 15	+2.518	stain HIGH 4/12	HPA011191	↓	

NOTE: This table lists the 29 significantly changing proteins between G3E and G4E, and their associated networks. Proteins selected for IHC evaluation are indicated in bold.

quality of staining achievable with said antibody. Following this analysis, it was found that 26 of the 29 proteins had available antibodies of high quality. At this point, observations made during the IPA network analysis—which provided information on the functional role of the proteins of interest—were considered to further prioritize the protein selection for IHC-based evaluation. Ultimately, four proteins were selected based on (i) their observed fold change between G3E and G4E, (ii) the quality of antibody available for them, and (iii) their association (if any) with functional networks. Two of proteins that are upregulated between G4 and G3 epithelia—nucleolin (NCL) and U2 small nuclear ribonucleoprotein A (SNRPA1)—and two proteins that are downregulated—Ras-related protein Rab-3D (RABD3) and Bifunctional epoxide hydrolase 2 (EPHX2) were selected. The

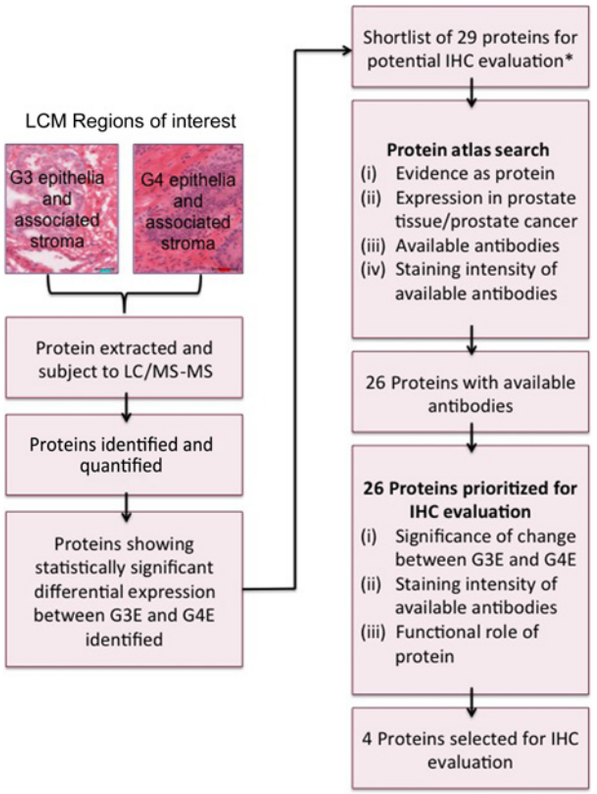

Figure 3.
Workflow for the prioritization of protein candidates for evaluation by IHC: *A shortlist of 29 proteins for potential IHC evaluation was compiled following multiple rounds of significance testing in Perseus software.

networks associated with these proteins (where applicable) are indicated in Table 3. The expression of these proteins was evaluated in tumor sections from 133 patient biopsy samples. For each individual patient tumor sample, three cores of specified regions of biopsied tissue—normal (N), Gleason grade 3 (G3), Gleason grade 4 (G4), and Gleason grade 5 (G5)—were stained for the expression of the four proteins. For the various biopsy ROIs, not all cores were viable for staining and so, the conclusions made based on this evaluation are strictly observational and based only on what viable tissue was available. Therefore, this evaluation provides limited information for which to draw any conclusions as to the potential use of these proteins are discriminatory markers between G3 and G4 tumors. Nevertheless, three of the four proteins—NCL, RABD3, and SNRPA1—appear to show an obvious change difference in expression between G3 and G4 tumors (Fig. 4B). Importantly, the proteins NCL and EPH appear to be differentially expressed in patients with G3+4 versus G4+3 prostate cancer (Fig. 4C)

Discussion

In this study, label-free LC-MS/MS analysis of distinct regions of G3 and G4 prostate cancer tumor was achieved. Changes in protein expression between G3 and G4 tumor tissues may be relevant to the varied clinical outcome for patients with G7 prostate cancer, which appears to be dependent on whether their tumor is mainly composed of G3 or G4 grade tissue. Such in-depth profiling of ROIs within the tumor microenvironment was made possible by coupling laser microdissection with a standardized workflow for LC-MS/MS analysis. To ensure sufficient tissue material for comprehensive proteomic profiling of regions of Gleason 3 and Gleason 4 prostate cancer, LCM was performed using patient samples that were rich in either Gleason 3 or Gleason 4 grade tumor tissue, i.e., patients with G6 (G3+3) or G8 (G4+4) prostate cancer. LCM and its application to downstream analytical methodologies have been reviewed extensively (21). However, since the development of LCM, its use for the isolation of cellular material suitable for large-scale, comprehensive proteomic analysis has lagged behind in comparison to its application to other "omics" approaches. This is primarily due to the unavoidably limited amount of sample routinely acquired using LCM and the relatively large amounts of material required for proteomic analyses. With the recent development of more sensitive and sophisticated mass spectrometric instrumentation (28–30), several groups have used mass spectrometry to undertake extensive proteomic analysis with as little as a few thousand cells (31). As such, the possibility of conducting extensive proteomic analysis of a limited number of cells obtained (by LCM) from discrete tissue regions is now a highly attractive and increasingly feasible strategy for biomarker discovery (32–35). There are two distinct obstacles in relation to carrying out such large-scale global proteomic analysis of the tumor microenvironment. First, LCM requires accurate identification of the target cells and hence microdissection of malignant or premalignant lesions requires the guidance of an expert pathologist for the definitive identification of cellular subtypes within the tissue/lesion field. Second, the time and effort required to obtain adequate cellular material for proteomic analysis using LCM can be a significant impediment to the design and implementation of suitably sized experiments (36).

Through application of a micropathologic approach, LCM was used here to successfully and efficiently isolate regions of G3 epithelia and stromal tissue and G4 epithelia and stromal tissue for advanced LC-MS/MS-based proteomic analysis. Comprehensive proteomic profiling of ROIs led to a number of interesting observations. It was observed that there were more significantly changing proteins between the epithelial and stromal tissues in G4 tumor as compared with G3 tumor. This may reflect an increase in cellular signaling activity that could be associated with the more aggressive nature of tumors that have a greater proportion of G4 tumor tissue. Indeed, pathways associated with cell-to-cell signaling, cell death and survival, and protein synthesis were found to be upregulated in the stroma of G4 tumor, whereas activation of pathways regulating cell morphology and cellular assembly and organization were observed to be upregulated in the G3 stroma. Within the microenvironment of both G3 and G4 tumors, differential regulation of various pathways was observed between epithelial and stromal tissues (Table 3). In this instance, we focused our interest on those proteins and pathways that show differential regulation between G3 and G4 epithelial tissues. From analysis of the LC-MS/MS data generated in this study, we have observed that the differences between G3 and G4 epithelia are subtle but, based on what we now understand of the prognoses for G3+4 and G4+3 tumors, these changes are likely to be very

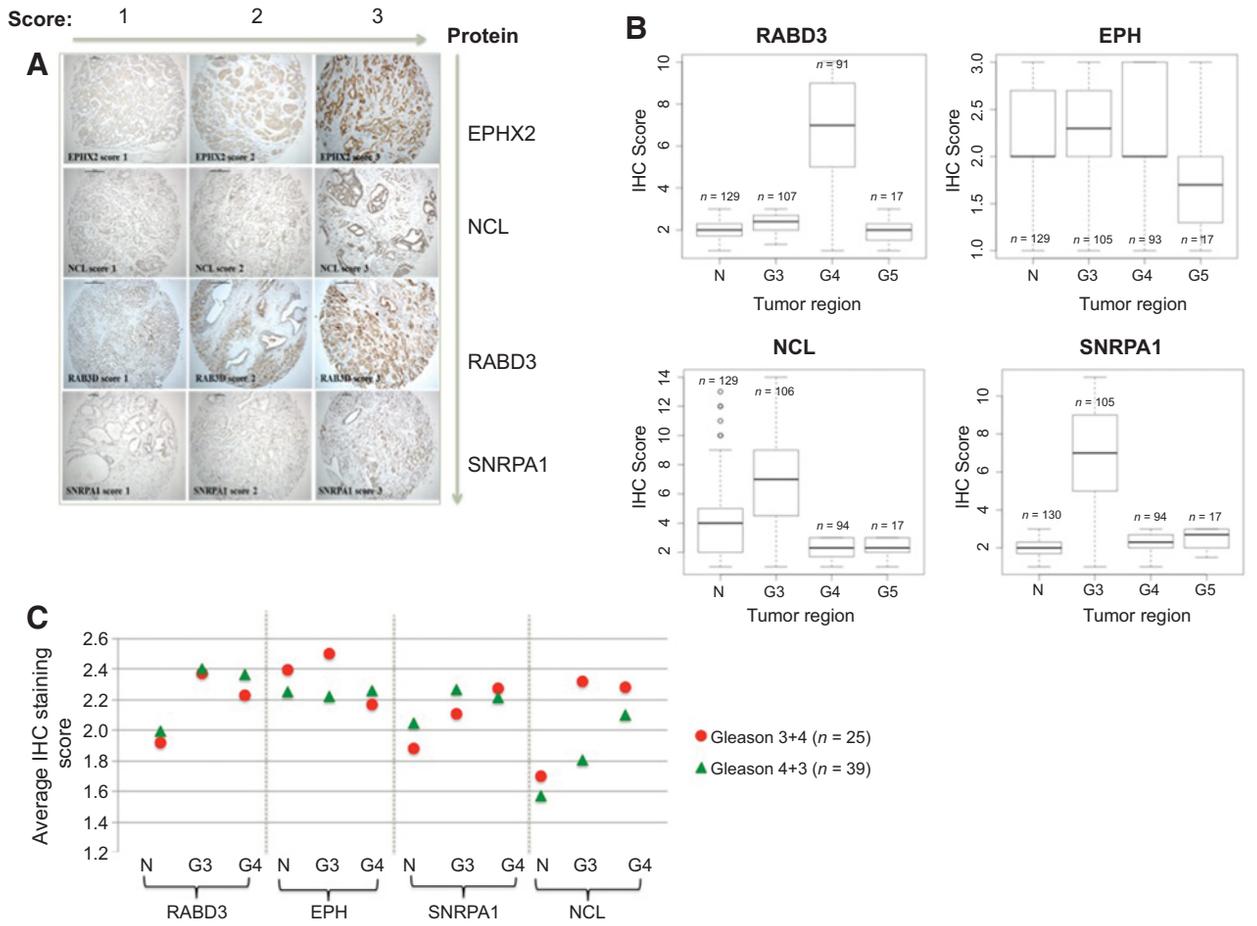

Figure 4.

IHC-based evaluation of proteins of interest. Tumor sections were incubated with primary antibodies at room temperature, followed by polyclonal rabbit anti-rat/anti mouse antibodies (Dako). For semiquantitative analysis, slides were scored 1 to 3 in normal prostatic tissue and various grades of prostatic adenocarcinoma (**A**). Box plots show the expression of the four proteins in regions of tumor tissue, as judged by the staining score for all available samples for each tumor region of interest (**B**). The Scatter plot shows the averaged expression of the four proteins in tumor regions from G3+4 and G4+3 patients (**C**).

important. Indeed, within the sample cohort used for IHC analysis, incidence of biochemical recurrence was much greater in patients with G4+3 prostate cancer than for patients with G3+4 prostate cancer (Supplementary Fig. S3, Supplementary Table S3) The observed molecular differences warrant further investigation and so a number of proteins were selected for evaluation by IHC.

Of the complete list of 29 proteins that are consistently differentially expressed between G3 and G4 epithelia, four were selected for evaluation following a stringent selection process (Fig. 3). This process, which intuitively availed of data available from an online repository—Protein Atlas—allowed selection of the highest quality antibodies to select those proteins for which we would have the greatest potential to generate an accurate measurement of protein expression. The proteins selected here were nucleolin, U2 small nuclear ribonucleoprotein A (upregulated in G4E vs. G3E), Ras-related protein Rab-3D, and Bifunctional epoxide hydrolase 2 (downregulated in G4E vs. G3E).

Nucleolin is the major nucleolar protein of growing eukaryotic cells. Due to its multifunctional features and localization in several cellular compartments, nucleolin is a key mediator of cell transformation and a key promoter of cell proliferation (37). The role of nucleolin has been investigated heavily in a number of cancer types. For example, it has been shown that increased expression of nucleolin correlates strongly with poor prognosis for patients with hepatocellular carcinoma (HCC; ref. 38). Further studies have strengthened the case for use of nucleolin as a marker for invasive HCC progression and suggest it may have role in the process of transcriptional elongation (39). It has also been shown that nucleolin positively regulates EGFR stability by binding to and interacting with EGFR mRNA, thereby promoting EGF-induced malignant cell transformation and migration (40). Nucleolin levels have also been associated with DNA damage repair and so may serve as a potential biomarker of treatment outcome (41). Recent work has suggested a link between nucleolin expression and the stem cell–like phenotype in breast cancer and so the potential of cell surface nucleolin as a target receptor in breast CSC for intracellular delivery of proapoptotic C6-ceramide and doxorubicin has been investigated, with promising results so far (42). In addition, studies indicate that nucleolin may be an

effective treatment target for patients with non–small cell lung cancer (NSCLC), and there is currently a phase II clinical trial underway to assess AS1411-targeted nucleolin for the treatment of metastatic NSCLC (43). To date, it has been shown that AS1411 has an excellent safety profile and has stabilized disease progression in numerous cases without any dramatic or long-lasting ill effects (44). Other ligands which cell surface nucleolin, such as endostatin and pseudopeptide N6, have also been used to block tumor growth and angiogenesis (45).

U2 small nuclear ribonucleoprotein A is known to be associated with U2 spliceosomal RNA. The relevance of RNA splicing in cancer is rapidly emerging, as demonstrated by spliceosome mutations that associate with prognosis of patients with breast cancer (46). Indeed, there are data to suggest that MYC-driven breast cancers are sensitive to modest perturbations in spliceosome function (47). There is even evidence to suggest that spliceosome modulation is a valid target for cancer therapy (48). Bifunctional epoxide hydrolase 2 is a bifunctional enzyme with a role in xenobiotic metabolism. Although it has not yet been reported to have an association to cancer, it does have a role in the regulation of cardiovascular and renal physiology (49). Less is known about the Ras-related protein Rab-3D protein other than that it has a role in protein transport—most likely in the regulation of exocytosis.

The IHC-based evaluation of these proteins was undertaken on biopsy samples from 133 prostate cancer patients. From each patient tissue block, three cores were taken from regions of normal tissue and G3, G4, or G5 tumor—depending on their individual tumor grades. Unfortunately, this evaluation strategy was restricted by the limited availability of viable tissue, and so it was not always possible to stain three cores for each of the target tissue regions from all patient tissue blocks (Supplementary Table S3). As such, the conclusions to be drawn from this part of the study are highly subjective and merely highlight potential trends in expression of the selected proteins. For the proteins U2 small nuclear ribonucleoprotein A and nucleolin, there appeared to be an increase in expression in G3 as opposed to G4 tumor tissue Ras-related protein Rab-3D showed increased expression in G4 tumor (Fig. 4B). Importantly, two of the proteins identified based on differential expression between G3 and G4 tumor epithelium show differential expression in G3+4 versus G4+3 prostate cancer patient in the validation cohort (Fig. 4C). Another important observation made from this analysis was that the expression of all four proteins also showed variation in the "normal" tissue regions between individual patients (Supplementary Fig. S4). We postulate that this may be due to the fact that the molecular phenotype of "normal" prostate tumor is also affected based on its proximity to tumor tissue or its surrounding stromal tissue. Overall, these results further highlight the complexity and heterogeneity of the prostate cancer tumor microenvironment.

The lack of definitive results obtained from the IHC staining of prostate cancer patient biopsy samples could likely be due to poor antibody sensitivity or limited dynamic range which is inherent to the technique—as well as the limited amount of viable tissue available (50). Although IHC is widely used in contemporary pathology as a diagnostic and prognostic tool, it is now accepted that one of the major limitations associated with conventional IHC is the fact that results are usually obtained by visual qualitative or semiquantitative evaluation (51). In addition, frequent genetic differences between regions of individual tumors and limited tumor sampling by needle biopsy pose significant challenges to molecular-based IHC assays in prostate cancer (52). A recent article has suggested that universal application of defined cut-offs can achieve reasonable strength of agreement in practicing pathologists for scoring of immunostains (53). However, it is suggested that the "next generation" of IHC will incorporate advanced digital technologies to improve quantification and spatial and multiparametric analysis (51). As an example, Shipitsin and colleagues have developed and applied a robust quantitative multiplex proteomics imaging approach to identify and measure protein biomarker candidates of prostate cancer in a manner that is resistant to the sampling errors mentioned here. This approach is the basis for the ProMark assay and aims to achieve reproducible, simultaneous quantification of protein levels and functional activities in prostate cancer tumor tissue specimens (27, 54).

In addition, we can suggest a number of currently established and more advanced technologies that could be applied for accurate verification of protein biomarker expression in tissue. Multiplexed multiple reaction monitoring (MRM) methods have been very effectively applied for the assessment of prostate cancer biomarker panels of potential clinical relevance (55). "Stable isotope standards and capture by anti-peptide antibodies" (SISCAPA) is a technique that employs immunoaffinity enrichment of targeted peptides of proteins of interest from digested tissue or biofluids prior to analysis by MRM mass spectrometry (56). A study by Kuhn and colleagues confirmed that this is a valid technique for accurate measurement of a 4-protein signature of response to tamoxifen therapy in patients with recurrent ER-positive breast cancer, and that this MRM-based classifier can be used in both tissue and serum samples (57). Although this is a promising approach, the poor availability of monoclonal antibodies validated for immunoaffinity enrichment of proteotypic peptides and the cost and time required to develop such antibodies *de novo* restrict the ability to develop a large number of peptide immuno-MRM assays (58). Another technique that has been advocated for use in measuring tissue biomarkers is that of Matrix-assisted laser desorption/ionization-mass spectrometry imaging (MALDI-MSI). This technology can be used to localize molecules of interest in tissue sections in order to investigate their spatial and temporal distributions in organs or whole body. This is especially useful for complex diseases such as cancer where the boundary between tumor and normal tissue is not clear or when the separation of cancer tissue from normal tissue is difficult. This technology has been well established in drug distribution analysis; however, in terms of biomarker research, many of the proteins that are used as therapeutic or imaging targets are not usually present in high enough concentrations to be visualized by MALDI-MSI (59–61).

The key to successful biomarker discovery is defining a specific clinical question and designing an appropriate investigative approach to address this question. Within the field of proteomics, the Human Protein Atlas has recently mounted a proteome-wide quality control initiative to ensure that researchers have access to high quality datasets and thereby enhance future biomarker-focused research initiatives (62). With regard to prostate cancer, the degree to which novel biomarkers will influence patients' and physicians' treatment choices represents the true clinical impact of any emerging protein biomarker–based diagnostics assay (63). Take, for example, the ProMark assay which is used to supplement current biopsy-based prostate cancer risk assessment methods in cases where clinical decision-making is not straightforward. An

economic analysis conducted by Roth and colleagues led to the conclusion that this protein-based assay has the potential to improve quality of life for prostate cancer patients while reducing cost—even if the magnitude of health outcome benefits is modest (63). In this study, a clinically integrated strategy was undertaken to investigate the molecular differences between G3 and G4 prostate cancer tumors that can account for the recognized variances in prognoses for patients who receive a diagnosis of G7 prostate cancer. The rich protein dataset acquired in this study has indeed highlighted a number of proteins and pathways that are differentially regulated between G3 and G4 tumor epithelia. Although it would be advantageous to be able to profile a larger number of proteins, the data described here have led to the identification of a number of proteins that are worthy of further investigation. Specifically, nucleolin looks promising and merits further detailed interrogation for use as biomarker or potential therapeutic target. Further evaluation of this protein and others that were shown to have a significant change in expression between G3 and G4 epithelia may lead to the identification of biomarkers that have suitable discriminatory ability for classification of G3+4 and G4+3 prostate cancer. In conclusion, this MS dataset, in combination with complimentary RNAseq data, provides a strong foundation for future studies into the molecular profiling of G3+4 and G4+3 prostate cancer.

Disclosure of Potential Conflicts of Interest

S.R. Pennington has ownership interest (including patents) in, and is a consultant/advisory board member for, Atturos.com. No potential conflicts of interest were disclosed by the other authors.

Authors' Contributions

Conception and design: L. Liotta, M. Bowden, J. O'Leary, S.P. Finn, M. Loda, S.R. Pennington

Development of methodology: L. Staunton, L. Liotta, M. Bowden, J. O'Leary, M. Loda, S.R. Pennington

Acquisition of data (provided animals, acquired and managed patients, provided facilities, etc.): L. Staunton, V. Espina, M. Bowden, M. Loda

Analysis and interpretation of data (e.g., statistical analysis, biostatistics, computational analysis): C. Tonry, R. Inzitari, A. Fabre, S.R. Pennington

Writing, review, and/or revision of the manuscript: C. Tonry, R. Lis, L. Liotta, A. Fabre, S.P. Finn, S.R. Pennington

Administrative, technical, or material support (i.e., reporting or organizing data, constructing databases): R. Lis, S.R. Pennington

Study supervision: J. O'Leary, M. Loda, S.R. Pennington

Acknowledgments

The authors wish to thank Clyde Bango of the Center for Molecular Oncologic Pathology (DFCI) for his technical assistance and support. Mass spectrometry technical assistance from Kieran Wynne of the Mass Spectrometry Resource, UCD Conway Institute, is acknowledged. They also wish to thank the Pathological Society of Great Britain and Ireland for visiting fellowship to which Lisa Staunton was a recipient. Lastly, they thank the Irish Prostate Cancer Research Consortium for access to samples used in method optimization and the Gelb Center for patient samples used in this study.

Grant Support

The UCD Conway Institute and the Proteome Research Centre is funded by the program for research in Third Level Institutions, as administered by the Higher Education Authority of Ireland. Funding is also acknowledged from the Health Research Board (HRB; HRA_POR/2011/125).

The costs of publication of this article were defrayed in part by the payment of page charges. This article must therefore be hereby marked *advertisement* in accordance with 18 U.S.C. Section 1734 solely to indicate this fact.

Received October 16, 2016; revised December 11, 2016; accepted December 13, 2016; published OnlineFirst January 5, 2017.

References

1. Sun T, McKay R, Lee GSM, Kantoff P. The role of miRNAs in prostate cancer. Eur Urol 2015;68:589–90.
2. Blume-Jensen P, Berman DM, Rimm DL, Shipitsin M, Putzi M, Nifong TP, et al. Development and clinical validation of an in situ biopsy-based multimarker assay for risk stratification in prostate cancer. Clin Cancer Res 2015;21:2591–600.
3. Shah RB. Current perspectives on Gleason grading of prostate cancer. Curr Urol Rep 2011;12:216–22.
4. Humphrey PA. Gleason grading and prognostic factors in carcinoma of the prostate. Mod Pathol 2004;17:292–306.
5. The Prostate Cancer Complexity Working Group. Merging bottom-up and top-down approaches to study prostate cancer biology [Internet]. Complexity 2002;7:22–30. Available from: http://doi.wiley.com/10.1002/cplx.10036
6. Doshi C, Vacchio M, Attwood K, Murekeyisoni C, Mehedint DC, Badkhshan S, et al. Clinical significance of prospectively assigned Gleason tertiary pattern 4 in contemporary Gleason score 3+3=6 prostate cancer. Prostate 2016;76:715–21.
7. Epstein JI, Zelefsky MJ, Sjoberg DD, Nelson JB, Egevad L, Magi-Galluzzi C, et al. A contemporary prostate cancer grading system: A validated alternative to the Gleason score. Eur Urol 2015;69:428–35.
8. Hägglöf C, Bergh A. The stroma-a key regulator in prostate function and malignancy. Cancers (Basel) 2012;4:531–48.
9. Klein G. Evolutionary aspects of cancer resistance. Semin Cancer Biol 2014;25:10–4.
10. Engels B, Rowley DA, Schreiber H. Targeting stroma to treat cancers. Semin Cancer Biol 2012;22:41–9.
11. Webber JP, Spary LK, Mason MD, Tabi Z, Brewis IA, Clayton A. Prostate stromal cell proteomics analysis discriminates normal from tumour reactive stromal phenotypes. Oncotarget 2016;7:20124–39.
12. Blume-Jensen P, Berman DM, Rimm DL, Shipitsin M, Putzi M, Nifong TP, et al. Biology of human tumors development and clinical validation of an in situ biopsy-based multimarker assay for risk stratification in prostate cancer. Clin Cancer Res 2015;21:2591–600.
13. Emmert-Buck MR, Bonner RF, Smith PD, Chuaqui RF, Zhuang Z, Goldstein SR, et al. Laser capture microdissection. Science 1996;274:998–1001.
14. Li M, Peng F, Li G, Fu Y, Huang Y, Chen Z, et al. Proteomic analysis of stromal proteins in different stages of colorectal cancer establishes Tenascin-C as a stromal biomarker for colorectal cancer metastasis. Oncotarget 2016;7:37226–37.
15. De Marchi T, Braakman RBH, Stingl C, van Duijn MM, Smid M, Foekens JA, et al. The advantage of laser-capture microdissection over whole tissue analysis in proteomic profiling studies. Proteomics 2016;16:1474–85.
16. Oh WK, Hayes J, Evan C, Manola J, George DJ, Donovan M, et al. Development of an integrated prostate cancer research information system. Clin Genitourin Cancer 2006;5:61–6.
17. Laemmli UK. Cleavage of structural proteins during the assembly of the head of bacteriophage T4. Nature 1970;227:680–5.
18. Shevchenko A, Tomas H, Havlis J, Olsen J V, Mann M. In-gel digestion for mass spectrometric characterization of proteins and proteomes. Nat Protoc 2007;1:2856–60.
19. Rappsilber J, Ishihama Y, Mann M. Stop and go extraction tips for matrix-assisted laser desorption/ionization, nanoelectrospray, and LC/MS sample pretreatment in proteomics. Anal Chem 2003;75:663–70.
20. Staunton L, Tonry C, Lis R, Finn S, O'Leary J, Loda M, et al. Profiling the tumor microenvironment proteome in prostate cancer using laser capture

microdissection coupled to LC-MS—A technical report. EuPA Open Proteomics 2015;10:19–23.
21. Espina V, Wulfkuhle JD, Calvert VS, Vanmeter A, Zhou W, Coukos G, et al. Laser-capture microdissection. Nat Protoc 2006;1:586–603.
22. Karantza V. Keratins in health and cancer: More than mere epithelial cell markers. Oncogene 2011;18:1492–501.
23. Menon R, Panwar B, Eksi R, Kleer C, Guan Y, Omenn GS. Computational inferences of the functions of alternative/noncanonical splice isoforms specific to HER2+/ER−/PR− breast cancers, a chromosome 17 C-HPP study. J Proteome Res 2015;14:3519–29.
24. Katafigiotis I, Tyritzis SI, Stravodimos KG, Alamanis C, Pavlakis K, Vlahou A, et al. Zinc alpha 2-glycoprotein as a potential novel urine biomarker for the early diagnosis of prostate cancer. BJU Int 2012; 110:688–93.
25. Hale LP, Price DT, Sanchez LM, Demark-Wahnefried W, Madden JF. Zinc α-2-glycoprotein is expressed by malignant prostatic epithelium and may serve as a potential serum marker for prostate cancer. Clin Cancer Res 2001;7:846–53.
26. Jung WY, Sung CO, Han SH, Kim K, Kim M, Ro JY, et al. AZGP-1 immunohistochemical marker in prostate cancer: Potential predictive marker of biochemical recurrence in post radical prostatectomy specimens. Appl Immunohistochem Mol Morphol 2014;22: 652–7.
27. Shipitsin M, Small C, Choudhury S, Giladi E, Friedlander S, Nardone J, et al. Identification of proteomic biomarkers predicting prostate cancer aggressiveness and lethality despite biopsy-sampling error. Br J Cancer 2014; 111:1201–12.
28. Rose RJ, Damoc E, Denisov E, Makarov A, Heck AJR. High-sensitivity Orbitrap mass analysis of intact macromolecular assemblies. Nat Methods 2012;9:2–6.
29. Michalski A, Damoc E, Hauschild J-P, Lange O, Wieghaus A, Makarov A, et al. Mass spectrometry-based proteomics using Q Exactive, a high-performance benchtop quadrupole Orbitrap mass spectrometer. Mol Cell Proteomics 2011;10:M111.011015.
30. Scheltema RA, Hauschild J, Lange O, Hornburg D, Denisov E, Kuehn A, et al. The Q exactive HF, a benchtop mass spectrometer with a pre-filter, high performance quadrupole and an ultra- high field orbitrap analyzer. Mol Cell Proteomics 2014;10:1–29.
31. Wang N, Xu M, Wang P, Li L. Development of mass spectrometry-based shotgun method for proteome analysis of 500 to 5000 cancer cells. Anal Chem 2010;82:2262–71.
32. Li M, Xiao Z, Chen Y, Peng F, Li C, Zhang P, et al. Proteomic analysis of the stroma-related proteins in nasopharyngeal carcinoma and normal nasopharyngeal epithelial tissues. Med Oncol 2010;27:134–44.
33. Sugihara Y, Taniguchi H, Kushima R, Tsuda H, Kubota D, Ichikawa H, et al. Laser microdissection and two-dimensional difference gel electrophoresis reveal proteomic intra-tumor heterogeneity in colorectal cancer. J Proteomics 2013;78:134–47.
34. Fang X, Wang C, Balgley BM, Zhao K, Wang W, He F, et al. Targeted tissue proteomic analysis of human astrocytomas. J Proteome Res 2013;11: 3937–46.
35. Chang K-P, Yu J-S, Chien K-Y, Lee C-W, Liang Y, Liao C-T, et al. Identification of PRDX4 and P4HA2 as metastasis-associated proteins in oral cavity squamous cell carcinoma by comparative tissue proteomics of microdissected specimens using iTRAQ technology. J Proteome Res 2011;10:4935–47.
36. Hernández B, Parnell A, Pennington SR. Why have so few proteomic biomarkers "survived" validation? (Sample size and independent validation considerations). Proteomics 2014;14:1587–92.
37. Berger CM, Gaume X, Bouvet P. The roles of nucleolin subcellular localization in cancer. Biochimie 2015;113:78–85.
38. Guo X, Xiong L, Yu L, Li R, Wang Z, Ren B, et al. Increased level of nucleolin confers to aggressive tumor progression and poor prognosis in patients with hepatocellular carcinoma after hepatectomy. Diagn Pathol 2014; 9:175.
39. Qian B, Yao Y, Liu Y, Yan M, Huang Y, Chen Y. Nucleolin identified by comparative mass-spectra analysis is a potential marker for invasive progression of hepatocellular carcinoma. Mol Med Rep 2014;10: 1489–94.
40. Xie Q, Guo X, Gu J, Zhang L, Jin H, Huang H. p85α promotes nucleolin transcription and subsequently enhances EGFR mRNA stability and EGF-induced malignant cellular transformation. Oncotarget 2016;7: 16636–49.
41. Xu Z, Joshi N, Agarwal A, Dahiya S, Bittner P, Smith E, et al. Knocking down nucleolin expression in gliomas inhibits tumor growth and induces cell cycle arrest. J Neurooncol 2012;108:59–67.
42. Fonseca NA, Rodrigues AS, Rodrigues-Santos P, Alves V, Gregório AC, Valério-Fernandes Â, et al. Nucleolin overexpression in breast cancer cell sub-populations with different stem-like phenotype enables targeted intracellular delivery of synergistic drug combination. Biomaterials 2015;69:76–88.
43. Xu J, Lu S, Xu X, Hu S, Li B, Li WX, et al. Prognostic significance of nuclear or cytoplasmic nucleolin expression in human non-small cell lung cancer and its relationship with DNA-PKcs. Tumor Biol 2016; 37:10349–56.
44. Reyes-Reyes EM, Šalipur FR, Shams M, Forsthoefel MK, Bates PJ. Mechanistic studies of anticancer aptamer AS1411 reveal a novel role for nucleolin in regulating Rac1 activation. Mol Oncol 2015; 9:1392–405.
45. Benedetti E, Antonosante A, D'Angelo M, Cristiano L, Galzio R, Destouches D, et al. Nucleolin antagonist triggers autophagic cell death in human glioblastoma primary cells and decreased in vivo tumor growth in orthotopic brain tumor model. Oncotarget 2015; 6:42091–104.
46. Menon R, Im H, Zhang E, Wu SL, Chen R, Snyder M, et al. Distinct splice variants and pathway enrichment in the cell-line models of aggressive human breast cancer subtypes. J Proteome Res 2014; 13:212–27.
47. Hsu TY, Simon LM, Neill N, Marcotte R, Bland CS, Echeverria G V, et al. The spliceosome is a therapeutic vulnerability in MYC-driven cancer. Nature 2015;525:384–8.
48. Kashyap MK, Kumar D, Villa R, La Clair JJ, Benner C, Sasik R, et al. Targeting the spliceosome in chronic lymphocytic leukemia with the macrolides FD-895 and pladienolide-B. Haematologica 2015; 100:945–54.
49. Newman JW, Morisseau C, Harris TR, Hammock BD. The soluble epoxide hydrolase encoded by EPXH2 is a bifunctional enzyme with novel lipid phosphate phosphatase activity. Proc Natl Acad Sci U S A 2003;100:1558–63.
50. DeMarchi T, Kuhn E, Carr SA, Umar A. Antibody-based capture of target peptides in multiple reaction monitoring experiments. Methods Mol Biol 2015;1293:1–49.
51. Laurinavicius A, Plancoulaine B, Herlin P, Laurinaviciene A. Comprehensive immunohistochemistry: Digital, analytical and integrated. Pathobiology 2016;83:156–63.
52. Klein EA, Cooperberg MR, Magi-Galluzzi C, Simko JP, Falzarano SM, Maddala T, et al. A 17-gene assay to predict prostate cancer aggressiveness in the context of gleason grade heterogeneity, tumor multifocality, and biopsy undersampling. Eur Urol 2014;66:550–60.
53. de Geus SWL, Boogerd LSF, Swijnenburg R-J, Mieog JSD, Tummers WSFJ, Prevoo HAJM, et al. Selecting tumor-specific molecular targets in pancreatic adenocarcinoma: Paving the way for image-guided pancreatic surgery. Mol Imaging Biol 2016;18:807–19.
54. Shipitsin M, Small C, Giladi E, Siddiqui S, Choudhury S, Hussain S, et al. Automated quantitative multiplex immunofluorescence in situ imaging identifies phospho-S6 and phospho-PRAS40 as predictive protein biomarkers for prostate cancer lethality. Proteome Sci 2014; 12:40.
55. Kim Y, Jeon J, Mejia S, Yao CQ, Ignatchenko V, Nyalwidhe JO, et al. Targeted proteomics identifies liquid-biopsy signatures for extracapsular prostate cancer. Nat Commun 2016;7:11906.
56. Kuhn E, Whiteaker JR, Mani DR, Jackson AM, Zhao L, Pope ME, et al. Interlaboratory evaluation of automated, multiplexed peptide immunoaffinity enrichment coupled to multiple reaction monitoring mass spectrometry for quantifying proteins in plasma. Mol Cell Proteomics 2012;11: M111.013854.
57. De Marchi T, Kuhn E, Dekker LJ, Stingl C, Braakman RBH, Opdam M, et al. Targeted MS assay predicting tamoxifen resistance in estrogen-receptor-positive breast cancer tissues and sera. J Proteome Res 2016; 15:1230–42.
58. Schoenherr RM, Zhao L, Ivey RG, Voytovich UJ. Technical Brief commercially available antibodies can be applied in quantitative multiplexed

peptide immunoaffinity enrichment targeted mass spectrometry assays. Proteomics 2016;1–15.
59. Steurer S, Borkowski C, Odinga S, Buchholz M, Koop C, Huland H, et al. MALDI mass spectrometric imaging based identification of clinically relevant signals in prostate cancer using large-scale tissue microarrays. Int J Cancer 2013;133:920–8.
60. Bonnel D, Longuespee R, Franck J, Roudbaraki M, Gosset P, Day R, et al. Multivariate analyses for biomarkers hunting and validation through on-tissue bottom-up or in-source decay in MALDI-MSI: Application to prostate cancer. Anal Bioanal Chem 2011;401:149–65.
61. Cazares LH, Troyer D, Mendrinos S, Lance RA, Nyalwidhe JO, Beydoun HA, et al. Imaging mass spectrometry of a specific fragment of mitogen-activated protein kinase/extracellular signal-regulated kinase kinase kinase 2 discriminates cancer from uninvolved prostate tissue. Clin Cancer Res 2009;15:5541–51.
62. Omenn GS, Lane L, Lundberg EK, Beavis RC, Overall CM, Deutsch EW. Metrics for the human proteome project 2016: Progress on identifying and characterizing the human proteome, including post-translational modifications. J Proteome Res 2016;15:3951–60.
63. Roth JA, Ramsey SD, Carlson JJ. Cost-effectiveness of a biopsy-based 8-protein prostate cancer prognostic assay to optimize treatment decision making in gleason 3+3 and 3+4 early stage prostate cancer. Oncologist 2015;20:1355–64.